

# Discreteness-induced resonances and AC voltage amplitudes in long one-dimensional Josephson junction arrays

A. E. Duwel<sup>a</sup>, Shinya Watanabe<sup>b</sup>, E. Trías,  
T. P. Orlando<sup>a</sup>, Herre S. J. van der Zant<sup>c</sup>, and Steven H. Strogatz<sup>d</sup>

<sup>a</sup>Dept. of Electrical Engineering & Computer Science, M.I.T., Cambridge, MA, 02143, USA

<sup>b</sup>Cent. for Chaos & Turbulence Studies, Niels Bohr Institute, Blegdamsvej 17, Copenhagen, 2100, Denmark

<sup>c</sup>Dept. of Applied Physics, Delft University of Technology, P.O. Box 5046, 2628 C J Delft, The Netherlands

<sup>d</sup>Dept. of Theoretical & Applied Mechanics, Cornell University, Kimball Hall, Ithaca, NY, 14853, USA

to appear in the Journal of Applied Physics, autumn, 1997

## Abstract

New resonance steps are found in the experimental current-voltage characteristics of long, discrete, one-dimensional Josephson junction arrays with open boundaries and in an external magnetic field. The junctions are underdamped, connected in parallel, and DC biased. Numerical simulations based on the discrete sine-Gordon model are carried out, and show that the solutions on the steps are periodic trains of vortices, phase-locked by a finite amplitude radiation. Power spectra of the voltages consist of a small number of harmonic peaks, which may be exploited for possible oscillator applications. The steps form a family that can be numbered by the harmonic content of the radiation, the first member corresponding to the Eck step. Discreteness of the arrays is shown to be essential for appearance of the higher order steps. We use a multimode extension of the harmonic balance analysis, and estimate the resonance frequencies, the AC voltage amplitudes, and the theoretical limit on the output power on the first two steps.

85.25 Am, 85.25 Cp, 74.50

## I. INTRODUCTION

Josephson junction systems have a natural application as millimeter- and submillimeter-wave oscillators. To facilitate their use, however, ongoing research must address several issues. To produce oscillators with narrow linewidths and high power, we must study the harmonic content and oscillation amplitudes of Josephson sources. Furthermore, the conditions under which many Josephson oscillators can be phase-locked to produce higher output power continue to challenge researchers.

AC power has been measured from both continuous long Josephson junctions and discrete arrays of short junctions. In underdamped Josephson systems, the AC oscillation amplitudes are expected to be largest at certain resonant frequencies. Much analytical work has been done to predict the frequency of these resonances. The success of these analyses can be assessed by studying the DC current-voltage ( $I\{V$ ) characteristics. Steps appear in the  $I\{V$  when increases of the current bias over a certain range do not produce increases in the DC voltage. Instead, the input power drives large-amplitude AC oscillations. The frequency of these oscillations is related to the DC voltage by the Josephson relation,  $\hbar\omega = 2eV$ , where  $\hbar$  is the reduced Planck constant, while the spatial wavenumber is determined by the applied magnetic field,  $k = 2\pi f/\lambda$ , where  $f$  is the applied flux per unit cell normalized to  $\Phi_0$ . The oscillations can be approximated as the normal modes to the linearized system. This approach has been used successfully to predict resonance frequencies, or steps in the  $I\{V$  characteristics of many different geometries of Josephson systems. The dependence of the step voltage on applied magnetic field can be included, thus giving a dispersion relation for the associated oscillations. In the discrete case, the dispersion relation is nonlinear, and higher modes waves are expected to produce distinct steps in the  $I\{V$  [1,2]. One of the limitations of these linear analyses is that the predicted oscillations are necessarily single-harmonic, since the normal modes of the linearized Josephson system are simply Fourier modes. In addition, the absence of a driving force in the linearized system precludes any calculation of the oscillation amplitudes.

In order to predict oscillation amplitudes and the distribution of power among excited modes, the nonlinearity in the system must be more carefully treated. Perturbation techniques [3,4] clarify the role of the nonlinearity in driving the resonance and have been used to predict step voltages in Josephson systems. Combined with an appropriate ansatz, they also provide expressions for the oscillation amplitude [5-7]. However, analytic expressions for the AC amplitudes so far include only the first harmonic and are implicit [5].

In this paper we use experiments, simulations, and non-linear analysis to investigate the properties of discrete, planar arrays of Josephson junctions connected in parallel. Both experiments and simulations yield several resonant steps in the  $I\{V$ . Simulations indicate that on these steps, a traveling wave pattern dominates the oscillations of junctions in the array. In contrast to the linear picture, these resonances correspond to excitations of more than one

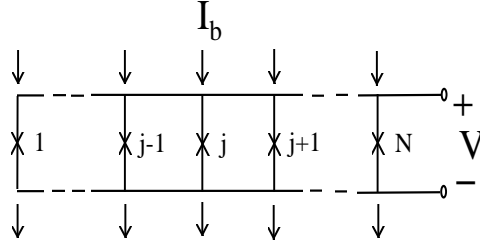


FIG. 1. Schematic of an open-ended parallel array. A uniform current  $I_b$  is applied at each of the upper nodes and extracted at the lower nodes.

mode, though the harmonic content is still limited. Similar states have already been reported in discrete rings [8], indicating that boundary conditions play a minor role. In inductively coupled arrays with open ends, the second harmonic resonance was also observed experimentally [9]. We use a two-mode extension of the harmonic balance method to predict the resonant frequencies as well as the mode amplitudes at resonance. Our formulas are analytic and include the dependence on magnetic field. With a matched load condition, a theoretical upper limit on the available output power of the underdamped Josephson oscillator is calculated.

## II. MEASUREMENTS OF ARRAYS

We have measured single-row arrays of  $N = 54$  junctions connected in parallel. Figure 1 shows a schematic of our device. A bias current  $I_b$  is applied at each upper node of the array and extracted from each bottom node as shown. We use resistors to distribute the bias current as evenly as possible. The voltage across the array is measured at an edge. The array is placed above a superconducting ground plane, and a separate control line (not shown) is used to apply a magnetic field. We will discuss the applied field in terms of the frustration,  $f$  (the flux applied to a single loop of the array, normalized to the flux quantum). Because the system is discrete, we expect its properties to be periodic in  $f$  with period  $f = 1$  [10]. In this experiment, the applied flux is proportional to the control current.

Samples were fabricated using a Nb trilayer process [11]. The junctions are  $3 \times 3 \text{ } \mu\text{m}^2$  with a critical current density of  $j_c(T = 0) = 1270 \text{ A}/\mu\text{m}^2$ . Device parameters have been determined using the diagnostic procedures described by van der Zant et al. [12]. For our samples at 7.2 K, the normal-state resistance  $R_n = 16.6 \text{ } \Omega$ , the self-inductance of a loop  $L_s = 6.4 \text{ pH}$ , the nearest-neighbor inductive coupling  $M_n = 0.11 L_s$ , the junction capacitance  $C = 340 \text{ fF}$ , and the Josephson inductance  $L_J = \phi_0 / (2 I_c) = 5.9 \text{ pH}$ . We use the normal-state resistance to calculate the Stewart-McCumber parameter,  $Q_c = 16$ . The sub-gap resistance is not as well defined at these high temperatures but approaches the value of  $R_n$ . For the discreteness parameter, we calculate  $\frac{2}{J} = L_J / L_s = 0.92$ .

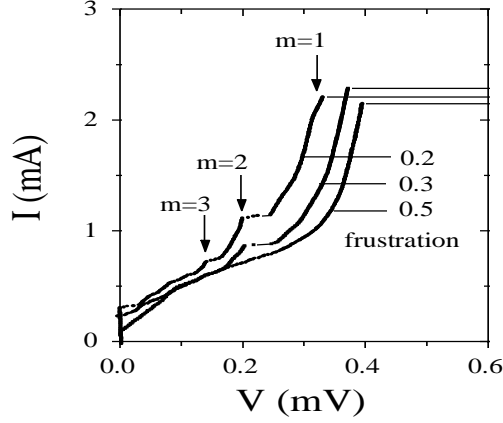


FIG. 2. Current vs. voltage of a 54-junction array on a ground plane at three values of  $f = 0.2; 0.3; 0.5$ . The temperature is 7.2K so that  $I_c R_n = 0.93 \text{ mV}$ . The three steps indicated by the arrows are labeled by  $m$  values corresponding the number of dominant harmonics in the  $m$  mode.

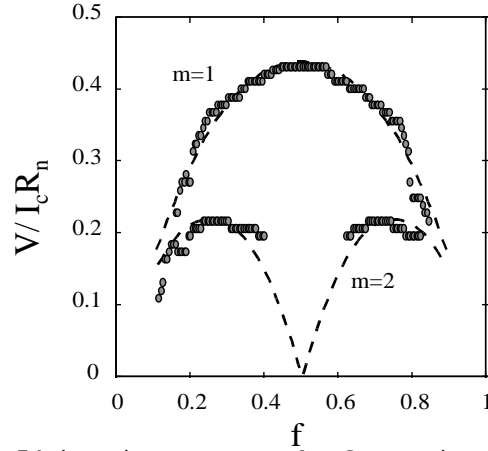


FIG. 3. Step voltages of the 54-junction array vs. the frustration,  $f$ , for the  $m$  modes  $m = 1$  and  $m = 2$ . The dashed curves are plots of Equation (13).

Figure 2 shows the voltage across an array when the current is uniformly injected. Three  $I\{V$  curves are presented, for  $f = 0.2, 0.3$ , and  $0.5$ . The most prominent feature is the sharp Eck step, which is the steepest part of the  $I\{V$ , just before the switch to the gap voltage (not shown). We label this step " $m = 1$ " for the reason given in the next section. In the regime where  $\gamma_c$  is small (overdamped) or  $\gamma_J$  is large (less discrete), this is the only step observed. For our underdamped and discrete samples, however, additional steps appear below the Eck voltage. We index these steps with  $m = 2; 3$ , etc. In this paper we are mostly concerned with the Eck step  $m = 1$  and, among the new steps, the clearest one with  $m = 2$ . The study of the second step sheds light on the other steps with  $m > 2$ .

The voltage locations of the peaks experimentally vary with  $f$ , as seen in Fig. 2. More systematically, we show the dependence of the first two steps in

Fig. 3. The Eck peak voltage is found to be periodic in  $f$  with period  $f = 1$  and to be approximately symmetric with respect to  $f = 0.5$ . This is consistent with previous observations [10]. At  $f = 0.5$ , the Eck step reaches its highest voltage value. For a smaller  $f$ , there is a threshold frustration, below which the Eck step does not appear. This cut-off  $f_{c1}$ , known as the lower critical field or frustration, is the minimum applied flux density for vortices to enter an array [10]. The value is quite large for our system,  $f_{c1} = 2 = (\frac{2}{\phi_J}) = 0.2$ . The voltage location of the second step shows roughly the same  $f$ -periodicity and symmetry as the Eck step. This second step, however, achieves the maximum voltage near  $f = 0.25$ , and it disappears near  $f = 0.5$  and for approximately  $f < f_{c1}$ .

The Eck ( $m = 1$ ) steps are ubiquitous in one-dimensional parallel arrays as well as in continuous long junctions. In contrast, the other steps ( $m > 1$ ) do not appear in long continuous junctions, but do appear in discrete arrays when  $\phi_J$  is small. In our arrays, we need  $\phi_J$  must be less than unity for the  $m = 2$  step to appear. Similar steps have been observed also in highly discrete circular arrays [8] and open-ended arrays consisting of two rows that are inductively coupled [5].

In open-ended arrays with a smaller  $N$ , Fiske steps [13] may be observed in a similar part of the  $I$ - $V$  below the Eck voltage. We emphasize, however, that they are qualitatively different. Fiske resonances can be described as standing waves (cavity modes) resulting from boundary reflections. The wavelength of the modes are restricted by the boundary geometry, and consequently, the resonance voltage locations do not depend strongly on  $f$ . At a certain value of  $f$ , only even or only odd modes are excited. As  $N$  becomes large, for a given value of damping, these Fiske resonances disappear due to damping of the edge reflections. None of these features apply for the Eck step as well as the  $m > 1$  steps, which are tunable in  $f$ . Thus, the new steps are expected to belong to the same family as the Eck step.

### III. SIMULATIONS

The governing equations which model our arrays are derived by applying Kirchhoff's current laws and using the RSJ model for the current through a single junction. We normalize the current to  $I_c$ , the voltage to  $I_c R_n$ , and time to  $\frac{\phi_J}{I_c C}$  (inverse plasma frequency). The equations are given in terms of the gauge-invariant phase differences across the junctions,  $\varphi_j$ , where  $j = 1; \dots; N$  indexes the junction's position. For simplicity we neglect all the cell inductances except the self-inductance, which results in the damped, driven, discrete sine-Gordon model:

$$\ddot{\varphi}_j + \gamma \dot{\varphi}_j + \sin \varphi_j = I_b = I_c + \frac{2}{J} (\varphi_{j+1} - 2\varphi_j + \varphi_{j-1}) \quad (1)$$

for  $j = 1; \dots; N$  and  $\gamma = \frac{1}{2}$ . Our numerical code can include longer range inductances as necessary, up to the full inductance matrix [14]. However, our

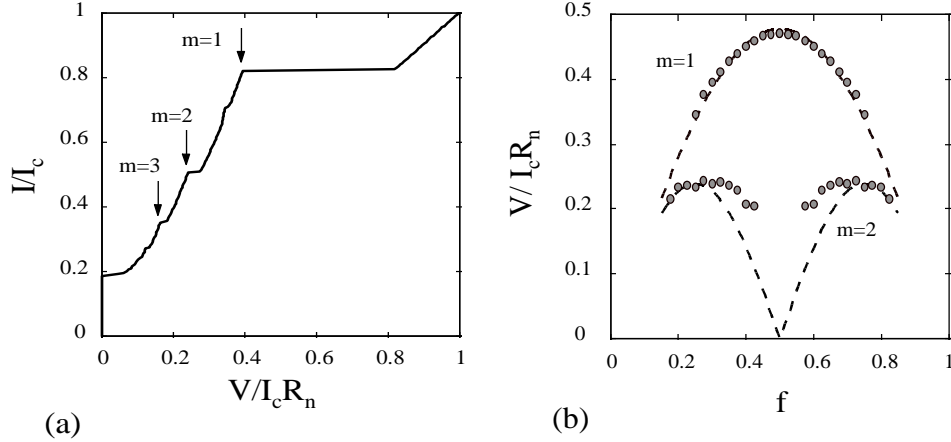


FIG. 4. (a) Simulated current-voltage characteristic for a 54-junction array at  $f = 0.3$ . The three most prominent steps are marked. (b) Voltages corresponding to the top of the steps show the tunability of the first two steps with magnetic field. The parameters are the experimental values:  $\phi_c = 16$  ( $\phi = 0.25$ ) and  $\frac{2}{J} = 0.92$ .

analysis in the next section uses mainly (1). Simulating the same equations allows us to make a direct comparison with our analysis. The simpler system not only illuminates the essential mechanism responsible for the observed steps but also reproduces the measurements reasonably well, as we will show in this section.

With only self-inductance, the boundary conditions are simply

$$\phi_0(t) = \phi_1(t) - 2\pi f \quad \text{and} \quad \phi_{N+1}(t) = \phi_N(t) + 2\pi f \quad (2)$$

for all  $t$ , where artificial junctions  $\phi_0$  and  $\phi_{N+1}$  are introduced at the endpoints so that (1) is valid at  $j = 1$  and  $N$  as well [15]. The fourth-order Runge-Kutta scheme with a time-step  $\Delta t = 1$  is used for integrating the system. The instantaneous voltage at junction  $j$  is simply proportional to the rate of the change of  $\phi_j$ , and is given in our normalization by

$$V = I_c R_n = d\phi_j/dt \quad (3)$$

With (1)-(3), current-voltage characteristics are numerically obtained at different  $f$  values using the parameters  $J$  and  $\phi$  from our experiments. Figure 4(a) shows the results for  $f = 0.3$ . The curve reproduces the measured one in Fig. 2 well, and at least three steps (indexed by  $m$ ) are clear. (There is also a small step just below the  $m = 1$  step which we think arises from a different mechanism.) In a manner similar to Fig. 3, the  $f$ -dependence of the step voltage locations is shown in Fig. 4(b). There are slight differences, but the main features and voltage values are represented well.

Simulations allow us to study the solutions in detail. We are especially interested in the system dynamics when biased on top of a step. In Fig. 5(a-c) the phase of the junction  $j = 27$  (located in the middle of the array) on the  $m = 1; 2; 3$  step, respectively, is shown as a function of time. The junction

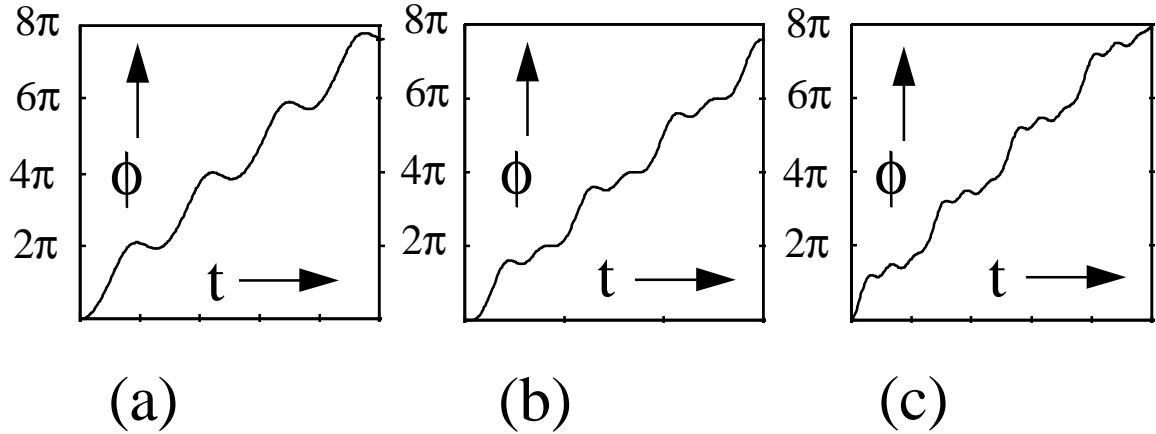


FIG. 5. Time evolution of the phase of a junction  $j = 27$  in the center of an array, biased on the (a)  $m = 1$ , (b)  $m = 2$ , and (c)  $m = 3$  steps, respectively. Note the increased frequency content as the mode number increases.

appears to be in a periodic motion. Its phase increases rapidly when a vortex (kink) passes by, and it oscillates for the period between passing vortices. In a mechanical analog of a junction as an underdamped pendulum [16], a sudden overturn of the pendulum is followed by an overshoot, and the pendulum "rings" several times until the next vortex passes by.

It appears in Fig. 5 that the solution on the step  $m$  corresponds to  $m$  such ringings. This can be quantified by studying the harmonic content of the voltages (3). Fourier spectra of the voltages are shown in Fig. 6(a-c), respectively. On the step  $m$ , the first  $m$  harmonics are dominant, and the higher harmonics have rapidly decaying magnitudes. Despite the presence of other harmonics, the steps are indexed by the ringing frequency,  $m$ .

Similar plots for the other junctions inside the array appear identical to  $j = 27$ , except for a certain shift in the time axis. This suggests that the solutions are well approximated by traveling waves. Near both ends of the array, reflections from the ends change this picture. The boundary effects, however, decay within 4-5 junctions from the end, and appear to play only a minor role in our long arrays.

Such traveling wave solutions, consisting of a vortex and ringing, have been found in circular arrays with the periodic boundary conditions [1,15,17]. In these systems, a vortex is trapped in a ring, and as it circulates, it creates an oscillatory wake, which phase-locks back to the vortex. It is not surprising that a nearly identical situation may arise in a linear array with open boundaries, if the array is sufficiently long. Instead of a single circulating vortex, a vortex lattice propagates through the array. A junction is swept periodically by a vortex in both cases. There is, however, one major difference between the two geometries. The magnetic field in the array (which controls the vortex spacing) can be continuously tuned in the linear geometry while it is restricted to multiples of  $\phi_0$  in a circular array due to the flux quantization.

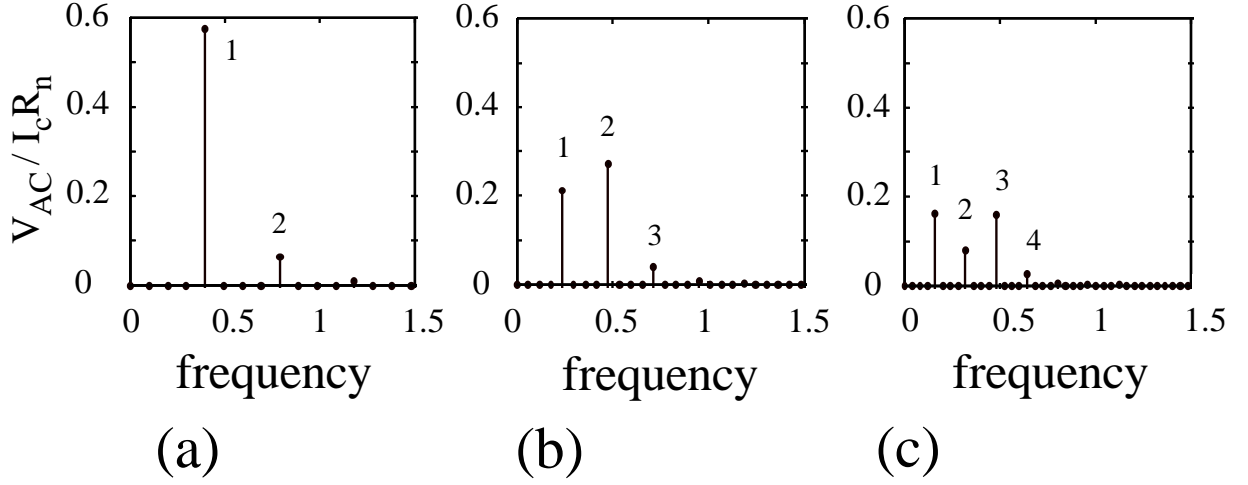


FIG. 6. Fourier spectra of the voltage corresponding to Fig. 5(a-c), with (a) step  $m=1$ , (b) step  $m=2$ , and (c) step  $m=3$ . Voltages are proportional to the time derivative of the phase in Fig. 5. The average slope of the phase plots corresponds to the DC voltage and is determined by the fundamental harmonic. The DC voltage was subtracted before computing the Fourier spectra. Note that only  $m$  harmonics are dominant for the  $m$ th step.

#### IV. ANALYSIS

In this section we seek a more analytical description of the system, and estimate DC voltages at each step and the amplitudes of the AC voltage components. The simulations in the previous section suggest that finding traveling wave solutions to the governing equation (1) is the key to the estimates, but this task is not simple in practice.

The equation (1) may be viewed as a variation, in two respects, from the integrable sine-Gordon partial differential equation,

$$\phi_{tt} + \sin \phi = -\alpha \phi_x \quad (4)$$

which possesses traveling kink solutions as exact solutions. Firstly, (1) is no longer a conservative equation, as it includes the external drive (bias current  $I_b$ ) and the loss ( $-\gamma$ ) terms. The added terms also break the integrability and exact solutions are no longer known. A perturbation approach [18] in the conservative limit ( $I_b, \gamma \rightarrow 0$ ) has been developed to approximate a kink solution.

Secondly, the spatial derivative in (4) is discretized in (1). In general, nonlinear wave equations discretized on lattices may exhibit qualitatively different solutions from their continuous counterparts, and study of such discreteness-induced effects is an active current topic in its own right [19]. For sine-Gordon systems, in particular, (1) was studied by [20,21,19] without a loss term or a drive, and it was found that propagation of a kink introduces a background radiation which greatly influences the speed of the kink. As far as we are aware, however, there has been no attempt to estimate the amplitudes of the induced radiation, especially in the driven case.



Strunz and Elmer [17] recently transformed (1) into a system of coupled modal equations and pointed out that the superharmonic resonance leads to creation of the radiated waves. They expanded a traveling waveform into Fourier modes, which may not be the best expansion basis but is a convenient one. Since our Fourier spectrum in Fig. 6 shows only a small number of peaks, we may truncate most modes and still obtain reasonable predictions. With this goal in mind, we review the analysis of [17] in Sec. 4A. The coupling terms among modes are truncated and analyzed in Sec. 4B, and we estimate the AC voltage amplitudes on the steps. The available power from the array is then evaluated in Sec. 4C.

#### A. Resonance mechanism and voltages

We look for traveling wave solutions of the discrete sine-Gordon equation (1) of the form

$$\varphi_j(t) = \varphi(x) = x + \psi(x) \quad (5)$$

where

$$x = \varphi t + 2\pi f j \quad (6)$$

is the moving coordinate with the wave, and  $\varphi(x + 2\pi) = \varphi(x)$ . The fundamental frequency  $\varphi$  is proportional to the DC voltage through the Josephson voltage-phase relation (3) while the spatial wavenumber is imposed by the external field. If the modulation were absent ( $\psi = 0$ ), then the boundary conditions (2) would be satisfied exactly. Since  $\psi$  is not vanishing, they are satisfied only on average, and there should be a correction to (5). We neglect this boundary effect and will show that the simplification still leads to good estimates of the measurements and simulations. (In a circular array (2) is replaced by the periodic boundary conditions:  $\varphi_{j+N}(t) = \varphi_j(t) + 2\pi M$  where  $M$  is an integer [15]. There can be exact solutions of the form (5,6) with  $f = M/N$ .)

The periodic function  $\varphi$  can be expanded into Fourier modes

$$\varphi(x) = \sum_{m=-1}^{\infty} A_m e^{imx} \quad (7)$$

with  $A_{-m} = A_m^*$ . We set  $A_0 = 0$ , without loss of generality, by shifting the origin of time. The phase  $\varphi$  is an increasing function of  $x$ , but the nonlinear term  $\sin \varphi$  is  $2\pi$ -periodic and can be expanded as

$$\sin \varphi(x) = \sum_{m=-1}^{\infty} F_m e^{imx} \quad (8)$$

with  $F_{-m} = F_m^*$ . The coefficients  $F_m$  can be computed in terms of  $A_1, A_2, \dots$  from the usual Fourier-Bessel expansions, and therefore provide coupling among the modes. By substituting (5,7,8) into (1), we obtain a coupled system of modal equations.

$$(\gamma_m + i\alpha_m)A_m + F_m = 0 \quad (9)$$

where

$$\gamma_m = \alpha_m^2 - (\alpha_m)^2; \quad (10)$$

and

$$\alpha_m = 2\alpha \sin(m\pi f): \quad (11)$$

The index  $m = 1; 2; \dots$  for (9,11). In addition, the balance of the DC terms in (1) results in

$$I_b = I_c = \alpha + F_0: \quad (12)$$

The first term on the right hand side is proportional to  $\alpha$ , and hence to the DC voltage. This term describes the ohmic line in the  $I\{V$  plane. The second term is also a function of  $\alpha$  through the  $A_m$ 's, and describes the deviation of the  $I\{V$  curve from the ohmic line.

The superharmonic resonance [22] may occur in the algebraic system (9,12) and lead to the creation of resonant steps in the  $I\{V$  curve. For small  $\alpha$ , the magnitude of  $A_m$  would generically become large near  $\gamma_m = 0$ , that is, near

$$\alpha = \alpha_m = m; \quad m = 1; 2; \dots: \quad (13)$$

Then  $F_0$  also becomes large, and the  $I\{V$  deviates substantially from the ohmic line near these frequencies (or corresponding voltages). This argument neglects the dependence of the coupling terms  $F_m$  on the complex amplitudes  $A_m$ , but explains our measurements quite well. We plot (13) for  $m = 1; 2$  as dashed curves in Figs. 3 and 4(b). The agreement is good without a fitting parameter.

The right hand side of (13) is the phase velocity of the  $m$ th mode on the discrete lattice. The left hand side can be viewed as the vortex velocity. Then, the relation can be viewed as the phase-locking condition of the vortex velocity and the phase velocity of the  $m$ th mode [1,15]. In the absence of the coupling terms  $F_m$ , a resonance occurs when the vortex lattice moves at the same velocity as one of the modes. We note that these resonance frequencies  $\alpha$  are distinct for different  $m$  because of the sinusoidal dependence of the dispersion relation (11) on  $m$ . If the second order difference in (1) were replaced by the second spatial derivative as in (4), the dispersion relation would depend linearly on  $m$ , and the phase velocities of all the modes would be identical. Consequently, there would be only one vortex velocity that can excite modes, and we would observe only one resonance voltage. This explains why only the Eck step (among this type of step) is observed in a long continuous junction. In this sense, our observation of the  $m > 1$  steps is due to the discreteness of the system.

We also note that, in some parameter regime, the resonating modes may be sub-harmonics of the fundamental frequency. Sub-harmonic resonances of order  $n$  can be sought by generalizing (7) to

$$x = \sum_{m=1}^{\infty} A_m e^{imx=n} : \quad (14)$$

This is still a traveling wave but has an  $n$  times longer period. In a similar manner to the above discussion, one may expect resonances when

$$0 = \omega_m^2 - (m\omega)^2 \quad \text{i.e.} \quad \omega = n\omega_m \quad (15)$$

where

$$\omega_m = 2\pi \sin(2m\pi f/n) : \quad (16)$$

The resonances with  $m = 1$  and  $n = 1; 2; 3$  have been observed by Caputo et al. [23].

#### B. Amplitudes at resonances

There was no need to analyze the coupling terms  $F_m$  in the previous section to determine the resonant voltages, but it becomes necessary when the AC components  $A_m$  are wanted. These mode amplitudes are important information for possible oscillator applications because one can then estimate the power available from the device.

One way to calculate the amplitudes is to linearize the coupled modal equations (9) with respect to  $A_m$ . One would obtain a linear algebraic system with coupling between neighboring modes only. We have tried this approach, but the estimated magnitudes became too large to justify the linearization, and they did not agree well with the numerically obtained mode amplitudes.

Therefore, we have used another approximation that can cope with larger amplitudes. Since analysis of the modal equations in general appears formidable, we focus only on the steps  $m = 1$  and  $2$ , and make several approximations.

First, as we see in the spectra in Fig. 6(a,b),  $A_3$  and higher modes have much smaller magnitudes on these two steps, so they will be neglected. Then,

$$\begin{aligned} x &= x + (A_1 e^{ix} + c.c.) + (A_2 e^{2ix} + c.c.) \\ &= x + a_1 \sin(x + \phi_1) + a_2 \sin(2x + \phi_2) \end{aligned} \quad (17)$$

where

$$A_m = (i=2) a_m e^{i\phi_m} : \quad (18)$$

The harmonic balance method, which is commonly used for approximating a finite amplitude solution, would neglect  $A_2$  as well. Thus, the ansatz (17) can be thought of an extension of the method to a multi-harmonic case.

Including two harmonics, however, introduces coupling terms between them, and makes the problem substantially harder. By the Fourier-Bessel expansion, the coupling is expressed as

$$F_0 = \sum_{n=1}^{\infty} J_{(2n+1)}(a_1) J_n(a_2) \sin [n\omega_2 - (2n+1)\omega_1] \quad (19)$$

and

$$F_m = \sum_{n=2}^{\infty} J_{m-(2n+1)}(a_1) J_n(a_2) e^{i(n\omega_2 + (m-2n-1)\omega_1)} + \sum_{n=1}^{\infty} J_{m-(2n+1)}(a_1) J_n(a_2) e^{-i(n\omega_2 - (m+2n+1)\omega_1)} \quad (20)$$

for  $m \neq 0$ , and  $J_m$  are Bessel functions.

To make analytical progress we simplify the coupling by taking only the most dominant terms (for small  $a$ 's) and neglecting all the others. This results in

$$F_1 = \sum_{n=2}^{\infty} J_0(a_1) J_0(a_2); \quad F_2 = \sum_{n=2}^{\infty} J_1(a_1) J_0(a_2) e^{i\omega_1} : \quad (21)$$

The higher order Bessel functions  $J_2(a_1)$ ,  $J_3(a_1)$ , ... and  $J_1(a_2)$ ,  $J_2(a_2)$ , ... are neglected, which can be justified in the range, say,  $a_1 \ll 2$  and  $a_2 \ll 1$ . We substitute them into (9) for  $m = 1, 2$  and obtain

$$(J_0(a_1)=a_1)^2 = (\frac{a_1^2}{2} + \frac{a_1^4}{8}) = J_0^2(a_2); \quad \tan \omega_1 = \omega_1 : \quad (22)$$

and

$$(J_0(a_2)=a_2)^2 = (\frac{a_2^2}{2} + \frac{a_2^4}{8}) = J_1^2(a_1); \quad \tan(\omega_2 - \omega_1) = \omega_2 - \omega_1 : \quad (23)$$

It is convenient to think of  $\omega$  as the control parameter and determine  $a_1$ ,  $a_2$ ,  $\omega_1$  and  $\omega_2$ . The arguments of tangent are defined between 0 and  $\pi$ . As  $\omega$  increases from 0,  $\omega_1$  and  $\omega_2$  decrease monotonically, and changes sign from positive to negative at the resonance frequencies. Thus,  $\omega_1$  decreases from  $\pi/2$  to 0, with the crossover  $\omega_1 = \pi/2$  at  $\omega = \omega_1$ . Similarly,  $(\omega_2 - \omega_1)$  decreases from  $\pi/2$  to 0, and crosses  $\pi/2$  at  $\omega = \omega_2$ .

The amplitude equations of (22,23) are more complicated. It follows from (23) that  $a_2 = 0$  when  $a_1 = 0$ . That is, the second mode is excited only in the presence of the first mode. On the other hand, the first mode can be excited alone since  $a_1 > 0$  in (22) when  $a_2 = 0$ . The feedback from the second mode through  $J_0(a_2)$  in (22) is not essential when considering  $a_1$ .

To extract more information we make a further approximation. We first linearize the Bessel functions on the right hand sides, i.e.  $J_1(a_1) \approx a_1/2$  and  $J_0(a_2) \approx 1$ . (Consequently,  $F_1$  becomes independent of  $a_2$ , and the feedback from the second mode is neglected. Then, (22) reduces to the equations obtained through the method of harmonic balance [5].)

On the left hand sides of (22,23), the function  $J_0(a)=a$  is monotonically decreasing from 1 to zero as  $a$  increases from 0 to the first zero of  $J_0$ , which

is a  $\frac{2}{3}$ . Thus, for any  $\omega$ ,  $a$  can be found within 0 and  $\frac{2}{3}$ . Approximating the function crudely by  $J_0(a) = a - \frac{1}{2}a^2$  would make the range of  $a$  unbounded. This is not desirable near the resonances. We could include the next term from the expansion of  $J_0$ , but this would make the following algebra more complicated. Alternatively, we replace the function by another one which has the same asymptotic behavior as  $a \rightarrow 0$  and a bounded domain for  $a$ . We use

$$(J_0(a) = a)^2 - 1 = a^2 - 1 = 4: \quad (24)$$

This has a slightly different saturation amplitude at  $a = 2$  but overall the approximation is good; the error in  $a$  introduced by this replacement is less than 5% for  $a < 0.7$  and at most 20% when  $a$  saturates. In return for the error introduced at this stage, we obtain simple expressions for the amplitudes as

$$a_1 = (b_1^2 + 1 = 4)^{-1/2} \quad \text{and} \quad a_2 = (b_2^2 + 1 = 4)^{-1/2}; \quad (25)$$

where

$$b_1^2 = \frac{2}{3} + \frac{2}{3}\omega^2 \quad \text{and} \quad b_2^2 = 4\left(\frac{2}{3} + \frac{2}{3}\omega^2\right) = a_1^2; \quad (26)$$

Once the phases and amplitudes of the modes are determined, the instantaneous voltage is obtained from the time-derivative of (17). In our normalization,

$$V = I_c R_n = \frac{1}{2} [1 + a_1 \cos(x + \phi_1) + 2a_2 \cos(2x + \phi_2)]; \quad (27)$$

Thus, the DC voltage and the AC amplitude of the mode  $m$  are

$$V_{DC} = I_c R_n = \frac{1}{2} \quad \text{and} \quad V_{AC} = I_c R_n = \frac{1}{2} m a_m; \quad (28)$$

In Fig. 7, we compare the amplitude estimate with simulations. On the first two steps, the peak AC voltage amplitudes for the first two Fourier modes are obtained from simulations, shown as data points. The estimates of the resonance frequencies  $\omega = \omega_1$  and  $\omega_2 = 2$  from (13) are used. The theoretical curves show a reasonable agreement with the data on the Eck step. On the second step the comparison is worse, but the overall magnitude and  $f$ -dependence are estimated fairly, considering the several approximations made during the derivation.

The maximum AC voltage oscillation of the first mode on the Eck step is achieved at  $f = 0.5$ . The maximum of the second mode on the second step happens near the lower critical frustration ( $f = 0.2$ ). The vertical axes in Fig. 7 are shown in terms of AC voltages. Converted back to the amplitudes,  $a_1 < 1.75$  and  $a_2 < 0.4$  on the Eck step for  $0.2 < f < 0.8$ . This is thought to be within the validity of the assumptions. On the second step,  $a_1 < 1.8$  for  $0.15 < f < 0.45$ , but  $a_2$  exceeds unity when  $f < 0.25$ . The bending of the theoretical curves in (b) when  $f < 0.25$  may be attributed to the large predicted magnitude of  $a_2$ . Including terms involving  $J_1(a_2)$  in the modal equations would be necessary to make a better estimate in the region.

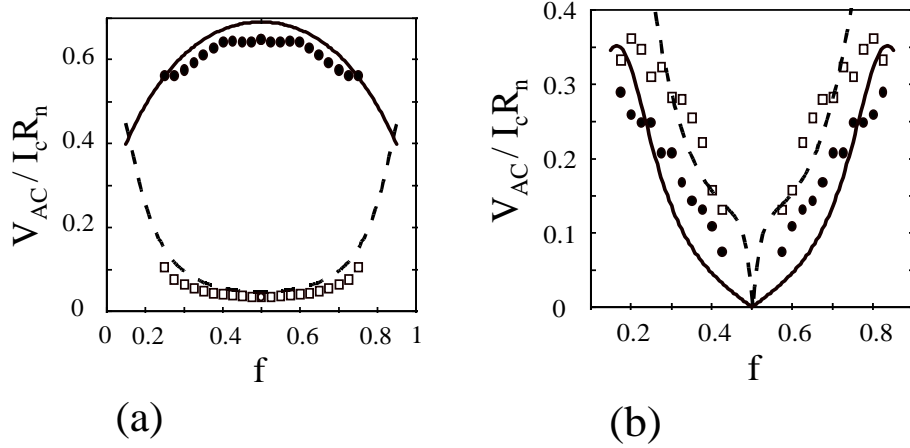


FIG. 7. Amplitudes of the first two AC voltage harmonics on (a) the  $m = 1$  (Eck) step and (b) the  $m = 2$  step vs.  $f$ . The theory (25) is represented by a solid (dashed) line for the first (second) harmonic. Filled circles and open squares show the amplitude of the first and second harmonics, respectively, from simulations. The values of  $\gamma$  and  $\beta$  are the same as in Fig. 4. As expected, the amplitude at the second frequency is quite small on the  $m = 1$  step (a), while the amplitudes of the first two harmonics are comparable on the  $m = 2$  step (b).

Generally, our assumption is violated when  $a_1$  saturates in (25), or when  $b_1^2$  becomes small. On the Eck peak  $b_1^2 = (2 - \gamma \sin(\pi f))^2$ , so the assumption breaks down for very small  $\gamma$  and/or  $\beta$ . Similarly,  $a_2$  exceeding unity indicates that we need more coupling terms included from (9). On the  $m = 2$  step,  $a_2 < 1$  is fulfilled when  $\beta^2 [1 + \beta^2 + 4(\beta_1^2 - \beta_2^2)^2] > 3 = 4$ . Again, small  $\gamma$  and/or  $\beta$  make it easier to violate the criterion. Thus, the validity of our approximations is limited to when  $\gamma$  is relatively large and resonances are not so strong.

### C. Power at resonances

The calculation of the mode amplitudes provides a theoretical upper limit for the power available from the Josephson oscillator at resonance. If we assume a matched load condition, then the power dissipated in the load is just the power dissipated in the matched resistance. Using the RSJ model and assuming sinusoidal voltage oscillations, this corresponds to  $P = V_{AC}^2 / 8R_{arr}$ , where  $R_{arr} = R_n / N$  is the array resistance. The power available from mode  $m$  is then

$$\frac{P_m}{I_c^2 R_n} = \frac{N}{8} \left( \frac{V_{AC}}{I_c R_n} \right)^2 = \frac{N}{8} (\beta a_m)^2 \quad (29)$$

with  $a_m$  estimated in (25). Therefore, the vertical axis of Fig. 7 is also  $\frac{P}{8P_m} = \frac{N}{I_c^2 R_n}$ , and the  $f$ -dependence of the powers can be read directly from the figure. When biasing on the Eck step, the largest power and the highest frequency are obtained at  $f = 0.5$ . When the system is biased on the second

step, the largest power is obtained near  $f = 0.2$ , and the highest frequency is achieved near  $f = 0.25$ .

We take our experimental values ( $I_c R_n = 0.93 \text{ mV}$  and  $R_n = 16.6 \text{ } \Omega$ ) and the maximum amplitudes in Fig.7 ( $V_{AC;1} = 0.65 I_c R_n$  on the Eck step and  $V_{AC;2} = 0.36 I_c R_n$  on the second step). This predicts a maximum of about 150 nW from the first harmonic at the first resonance and 46 nW from the second harmonic at the second resonance. These numbers are much smaller than previous estimates [24], and, according to measurements [25,26], are probably more realistic.

Our simulation and analysis show that multiple Fourier modes are excited on the new steps  $m > 1$ . For possible applications as oscillators, this is not desirable since the AC power is therefore distributed among the modes, instead of being concentrated in one mode, as at the Eck step. Usually in such a case one could simply increase the drive, to increase the output at the desired frequency. However, in this system the driving current is limited because if it is increased beyond the top of the step, the resonance becomes unstable. Furthermore, since the maximum output power is small for a single row, methods are needed to combine power from multiple rows while preserving the frequency content of the resonance.

Both discrete rows of underdamped Josephson junctions and continuous long junctions operating at the Eck step have already been proposed as high frequency oscillators [10,27]. Although no single experiment has directly compared the two systems, studies indicate that the output power levels are comparable, while the output impedance of the discrete system may be advantageously higher [10]. In order to increase power levels in either case, additional oscillators are required. Stacks of continuous long junctions have been fabricated and measured [28-30], as well as the analogous inductively coupled discrete arrays [5,9]. However, in both systems, the power is only increased if the oscillating elements are phase-locked and in-phase. The existence of in-phase as well as anti-phase states have been well established for both discrete and continuous systems, through numerics [31], simulations [2,32], and experiments [5,33]. Unfortunately, in both cases the anti-phase pattern is preferred at the Eck step [5,33], and the output oscillations of adjacent elements almost completely cancel. In addition, the difficulty (and necessity) of fabricating identical oscillators in the case of continuous stacks limits the possibility for improving this system.

On the other hand, the presence of higher harmonic resonances in discrete systems may actually be an advantage in terms of power combining. As observed in [9], when the discrete system is biased on the stable  $m = 2$  peak, the fundamental oscillations of the rows are anti-phase (shifted by  $\pi$ ), but the second harmonics are still in-phase. Thus, the output power from the second mode is enhanced. It is important to note that such modes do not exist in uniform continuous long junctions. So although the power level of a single row biased in this state is lower than the oscillators mentioned above, the potential for power-combining in this state is much greater. Simulations

indicate that this in-phase resonance for the second mode is stable for many coupled rows [9], which is promising for oscillator applications.

## V. SUMMARY

We have observed experimentally and through simulations new resonance steps in long one-dimensional Josephson junction arrays in the underdamped and discrete regime. They emerge in the  $I$ - $V$  characteristic below the Eck voltage, and are tunable in the magnetic field. We have shown that the resonance mechanism can be explained by neglecting the boundary effects and assuming a traveling wave solution. Fourier components of the solution resonate to create a waveform which appears to consist of a kink and radiation, phase-locked to each other. We have employed a two-mode extension of the harmonic balance method in order to simplify the coupling of the modes. We have derived an analytic formula for not only the resonance voltages but also the amplitudes of the modes. Finally, we used these results to predict the power available from such Josephson oscillators and discuss its dependence on the system parameters.

## ACKNOWLEDGMENT

We thank Mauricio Barahona, Alexey Ustinov, Andreas Wallra, and Pasquiline Caputo for valuable discussions. We acknowledge the support of the NSF Graduate Fellowship program and NSF Grants DMR-9402020, DMS-9057433, and DMS-9500948. We appreciate the partial support of the Dutch Foundation for Fundamental Research on Matter.



## REFERENCES

- [1] A. V. Ustinov, M. C. Cirillo, and B. A. Malmgren, *Phys. Rev. B* 47, 8357 (1993).
- [2] A. Petraglia and N. F. Pedersen, P. L. Christiansen, and A. V. Ustinov, preprint (1995).
- [3] S. Watanabe, S. Strogatz, H. S. J. van der Zant, T. P. Orlando, *Phys. Rev. Lett.* 74 (3), 379 (1995).
- [4] K. Yoshida, K. Hamasaki, and F. Irie, *Jap. J. Appl. Phys.* 18 (2), 373 (1979).
- [5] A. E. Duwel, E. Trias, T. P. Orlando, H. S. J. van der Zant, S. Watanabe, S. H. Strogatz, *J. Appl. Phys.* 79 (10), 7864 (1996).
- [6] I. O. Kulik, *Sov. Phys. JETP* 24, 1307 (1967).
- [7] K. Enpuku, K. Yoshida, and F. Irie, *J. Appl. Phys.* 52, 344 (1981).
- [8] H. S. J. van der Zant, T. P. Orlando, S. Watanabe, and S. H. Strogatz, *Phys. Rev. Lett.* 74, 174 (1995).
- [9] A. E. Duwel, T. P. Orlando, S. Watanabe, H. S. J. van der Zant, *Proc. Appl. Supercond. Conf.* (1996) to be published.
- [10] H. S. J. van der Zant and T. P. Orlando, *J. Appl. Phys.* 76 (11), 7606 (1994).
- [11] HYPERES, Inc., Elmford, NY 10523.
- [12] H. S. J. van der Zant, R. A. M. Reerveur, T. P. Orlando, A. W. Kleinsasser, *Appl. Phys. Lett.* 65 (16), 2102 (1994).
- [13] H. S. J. van der Zant, D. Berman, and T. P. Orlando, *Phys. Rev. B* 49 (18), 12945 (1994).
- [14] E. Trias, Master thesis, M. I. T., 1995.
- [15] S. Watanabe, H. S. J. van der Zant, S. H. Strogatz, and T. P. Orlando, *Physica* 97D, 429 (1996).
- [16] S. H. Strogatz, *Nonlinear Dynamics and Chaos*, pp. 106-113, Addison-Wesley Publishing Co. (1994).
- [17] T. Strunz and F. J. Elmer, in *Physics of Sliding Friction*, 149-161, (eds. B. N. J. Persson and E. Tosatti, Kluwer Acad. Pub., 1996).
- [18] R. D. Parmentier, in *The New Superconducting Electronics*, 221-248, Sec. 3.2, (eds. H. Weinstock and R. W. Ralston, Kluwer Acad. Pub., 1993) and references therein.
- [19] D. B. Duncan, J. C. Eilbeck, H. Feddersen, and J. A. D. Wattis, *Physica* 68D, 1-11 (1993).
- [20] M. Peyrard and M. D. Krukal, *Physica* 14D, 88-102 (1984).
- [21] R. Boesch, C. R. Willis, and M. El-Batanouny, *Phys. Rev. B* 40 (4), 2284-2296 (1989).
- [22] A. H. Nayfeh and D. T. Mook, *Nonlinear Oscillations*, Wiley-Interscience, New York (1979).
- [23] P. Caputo, A. V. Ustinov, N. Iosad, H. Kohlstedt, *J. Low Temp. Phys.* 106 N. 3/4, 353 (1997).
- [24] S. P. Benz, C. J. Burroughs, *Appl. Phys. Lett.* 58 (19), 2162 (1991).
- [25] A. V. Ustinov, H. Kohlstedt, P. Henne, *Phys. Rev. Lett.* 77 (17), 3617 (1996).
- [26] P. Booi, S. P. Benz, *Appl. Phys. Lett.* 64 (16), 21163 (1994).
- [27] N. F. Pedersen, A. V. Ustinov, *Sup. Sci. Tech.* 8, 389 (1995).
- [28] G. Carapella, G. Costabile, G. Filatella, M. H. Manscher, J. Mygind, N. A. Nordahn, N. F. Pedersen, A. Petraglia, *Proc. Appl. Supercond. Conf.* (1996) to be published.
- [29] A. V. Ustinov, H. Kohlstedt, C. Heiden, *Appl. Phys. Lett.* 65 (11), 1457 (1994).
- [30] S. Sakai, A. V. Ustinov, H. Kohlstedt, A. Petraglia, N. F. Pedersen, *Phys. Rev. B* 50, 12905 (1994).
- [31] N. Grnbech-Jensen, D. Cai, M. R. Samuelsen, *Phys. Rev. B* 48 (21), 16160 (1993).
- [32] S. Sakai, P. Bodin, N. F. Pedersen, *J. Appl. Phys.* 73 (5), 2411 (1993).
- [33] R. Monaco, A. Polcari, L. Capogna, *J. Appl. Phys.* 78 (5), 3278 (1995).